Published in final edited form as:
Biochemistry. 2013 August 27; 52(34): . doi:10.1021/bi400529q.

Comparison of diamine and Mg^{2+} interactions with RNA tertiary structures: similar vs. differential effects on the stabilities of diverse RNA folds

Robert J. Trachman III[1] and **David E. Draper**[*,1,2]

[1]Department of Biophysics, Johns Hopkins University, Baltimore, MD 21218

[2]Department of Chemistry, Johns Hopkins University, Baltimore, MD 21218

Abstract

Cations play a large role in stabilizing the native state of RNA *in vivo*. In addition to Mg^{2+}, putrescine^{2+} is an abundant divalent cation in bacterial cells, but its effect on the folding of RNA tertiary structure has not been widely explored. In this study, we look at how the stability of four structured RNAs, each with a different degree of dependence on K^+ and Mg^{2+}, are affected by putrescine^{2+} relative to Mg^{2+}. Through the use of thermal melts we observe that (i) at a given concentration, putrescine^{2+} is less effective than Mg^{2+} at stabilizing RNA; (ii) the stability imparted to RNA by various diamines is a function of charge density (average separation distance between charges) as well as flexibility of the counterion; and (iii) when Mg^{2+} is already present in a buffer, further addition of putrescine^{2+} may either destabilize or stabilize RNA structure, depending on whether the native RNA does or does not chelate Mg^{2+} ion, respectively. At ion concentrations likely to be found *in vivo*, the effect of putrescine^{2+} on the free energy of folding an RNA tertiary structure is probably quite small compared to that of Mg^{2+}, but the ability of mixed Mg^{2+} - putrescine^{2+} environments to (in effect) discriminate between different RNA architectures suggests that, in some cells, the evolution of functional RNA structures may have been influenced by the presence of putrescine^{2+}.

Introduction

The ionic composition of the cytoplasm plays a large part in dictating the stability of native RNA structure. In addition to the inorganic ions found in cells (predominantly K^+ and Mg^{2+}) organic cations such as putrescine^{2+} (1,4-diaminobutane) are found in concentrations high enough to warrant attention. (As putrescine is fully protonated near neutral pH, it will be referred to here as putrescine^{2+} when its cationic properties are being discussed.) Putrescine^{2+} is the third most abundant cation in bacterial cells with a total concentration that ranges between 10 and 60 mM in *E. coli*, depending on the growth medium (1). These levels are significant given that the most abundant divalent ion (Mg^{2+}) in the cell has a total concentration of ~100 mM (2). Despite the importance of understanding putrescine^{2+}-RNA interactions, relatively few studies have focused on this subject (3-5).

In this study, we seek to understand the significance of putrescine^{2+} ion in regard to RNA tertiary structure stability *in vivo*. We compare the efficacy of putrescine^{2+} and Mg^{2+} at stabilizing the tertiary structure of four different RNAs, chosen to be representative of the

[*]Corresponding author: Tel 410 516 7448. Fax 410 516 8420. draper@jhu.edu.

Supporting Information **Available:** Supporting information contains four figures showing the primary and secondary structures of the four RNAs used in this study, three additional melting curves for each RNA, and vapor pressure osmometry results for putrescine•2HCl. This material is available free of charge via the Internet at http://pubs.acs.org.

diversity of RNA folds found within a bacterial cell. The results are consistent in that Mg^{2+} stabilizes the native state of all four RNAs to a greater degree than the same concentration of putrescine^{2+}. In the presence of Mg^{2+}, the change in thermal stability upon addition of putrescine^{2+} is found to either increase or decrease depending on the fold of the RNA. These findings can be attributed to the inability of putrescine^{2+} to occupy Mg^{2+} chelation sites as well as a difference in charge density among different divalent cations. The unexpected ability of mixed Mg^{2+} - putrescine^{2+} solutions to stabilize or destabilize RNAs of different native architectures suggests that, in some cells, RNA structures have adapted to the presence of putrescine.

Materials and Methods

Chemicals and RNA

All solutions were prepared using water at 18.3 MΩ resistivity. All buffers and salts were ≥ 99.5% purity. MOPS buffer was obtained from Sigma, and brought to pH 6.8 with KOH (K•MOPS). The standard buffer was 40 mM K•MOPS (with 13 mM K^+) and 10 μM EDTA (Sigma). KCl (Fluka) was added to give the indicated total concentrations of K^+, e.g. 37 mM KCl to give 50 mM K^+. $MgCl_2$, and/or diamine were also added as indicated. (At pH 6.8, the diamines used in this study are all greater than 98% of the di-protonated species. . The relatively high concentration of K•MOPS was necessary to maintain pH 6.8 after additions of up to 10 mM of the HCl salts of the diamines used here.) Solutions of $MgCl_2$ (Fluka) were standardized by titration into an EDTA solution (pH 8.0) of known concentration, while monitoring absorbance at 230 nm (6).

The HCl salts of *cis*-1,4-diaminobutene and *trans*-1,4-diaminobutene were synthesized as described (7), and the products recrystallized twice from 1:1 methanol-ether. *Cis* and *trans* products were obtained in 70% and 58% yield, respectively and dried over phosphorus pentoxide. Proton NMR spectra recorded on a Bruker 400 confirmed the expected products; <1.5% of the total proton signal originated from unassigned peaks. The first acid dissociation constant (pK_a) of the 2HCl salts of putrescine, *cis*-1,4-diaminobutene and *trans*-1,4-diaminobutene were all determined by titration of the compound (at ~ 20 mM in 12 ml H_2O) with a standardized 100 mM KOH solution (25°C) while monitoring the pH with a calibrated Thermo Scientific, Ross combination 8102BN electrode.

All RNAs were prepared by transcription of linearized plasmid DNA with a histidine-tagged bacteriophage T7 RNA polymerase (8), as described (9). Transcription products were purified by preparative electrophoresis on denaturing, 9-12% polyacrylamide gels. The desired product band was excised from the gel, from which the RNA was electroeluted in an Elutrap Electrophoresis Chamber (Schleicher & Schuell). Centricon filter units (Millipore) were used to equilibrate an RNA in the desired buffer.

Vapor Pressure Osmometry

The osmolalities of putrescine•2HCl solutions were assessed by vapor pressure osmometry (VPO), using a Wescor VAPRO 5520 (Logan, UT) at ambient temperature. Solutions were prepared gravimetrically from dried, crystalline putrescine•2HCl and water. Osmolalities were measured three times on each sample and repeated four times with fresh stocks. Data were fit to a second order polynomial using Kaleidagraph, and compared with literature values for $MgCl_2$ (Figure S4). Putrescine•2HCl clearly deviates more strongly from ideal behavior than does $MgCl_2$ at concentrations greater than ~100 mmolal. The RNA stability measurements reported here use a mixture of divalent ion(s) and KCl/K•MOPS, the latter monovalent salts usually at a total of 50 mM and in excess over the concentration of Cl^- that accompanies the divalent ion. Under these conditions, the mean ionic activity coefficient of

the divalent cation is largely determined by the concentration of the anion. A good approximation is that the $MgCl_2$ mean ionic activity coefficient in experiments with 50 mM KCl is approximately the same as that of a $MgCl_2$ solution of the same ionic strength (10). (At I = 50 mM, or ~17 mM $MgCl_2$, $\gamma \approx 0.66$ (11).) In this region of Figure S4, the $MgCl_2$ and putrescine•2HCl osmolalities are identical within experimental error, and the limiting slopes of the fitted osmolality curves are also approximately the same (2.53 and 2.58).

Although the slope of the osmolality vs. molality curve is related to the activity of the solute, it is necessary to carry out an integration to obtain the activity coefficient. The equation is $\ln \gamma_2 = (\phi - 1) + \int [(\varphi - 1)/\varphi] dm_2$, where m_2 is the solute concentration, φ is the practical osmotic coefficient ($\varphi = Osm/m_2$), γ_2 is the mean ionic activity coefficient, and the integration is carried out from 0 to the m_2 concentration of interest (12)(13). The $(\varphi-1)$ term amplifies small errors at low molalities, and in addition the integrand approaches a non-zero value at zero solute concentrations. It is therefore necessary to have accurate measurements of osmolality at very low solute concentrations to obtain activities in the range of interest in these studies. VPO measurements are unable to quantify low solute osmolalities with sufficient accuracy, but we can estimate that about a three-fold lower osmolality for 25 mM putrescine•2HCl over 25 mM $MgCl_2$ would be necessary to generate even a factor of two difference in mean ionic activity coefficient. On this basis, we have compared the effectiveness of Mg^{2+} and putrescine^{2+} in stabilizing RNA in terms of their concentration, without introducing any correction for activity differences.

UV melting curves and melt data analysis

Thermal denaturation of RNA samples was carried out with either a Cary 400 spectrophotometer equipped with a six cell thermostatted cuvette holder or an Aviv model 14DS spectrophotometer with a five cell thermostatted cuvette holder. Each instrument was able to reproduce the results of the other within error. UV absorbance was variously monitored at 260, 280 and 295 nm. The temperature schedule for the experiments was as follows: heat from room temperature to 65°C, hold at 65°C for 5 minutes, cool to less than 10°C, then heat to 95°C. Temperature changes in the second and third stages was set between 0.5 and 0.66 °C/min. No significant hysteresis was observed between the cooling and second heating stages; we conclude that renaturation artifacts or RNA degradation has not biased the curves below 65 °C. Absorbance data were plotted as the derivative of absorbance with respect to temperature. The program Global Melt Fit was used to fit all resulting data and estimate errors by a bootstrap method (14). Global fitting of data collected at 260 and 280 nm was used to extract values for both T_m (melting temperature) and $\Delta H°$. The fitted enthalpies of a tertiary unfolding transition did not vary more than 7% over all the conditions tested; the average value was used in calculating $\Delta G°_{obs}$ at temperature T_0 from the formula

$$\Delta G^\circ(T_0) = \Delta H^\circ(T_0)(1/T_m - 1/T_0) \quad (3)$$

where T_0, the reference temperature, is 25 °C.

Plots of $\Delta\Delta G°_{obs}$, the difference between $\Delta G°_{obs}$ in the presence and absence of Mg^{2+} or putrescine, as a function of divalent ion concentration were fit to a Hill polynomial,

$$\Delta G^0_{obs} = (\Delta\Delta G^0_{obs,max}) \frac{([2+]/[2+]_0)^n}{(1+[2+]/[2+]_0)^n} \quad (4)$$

where $\Delta\Delta G°_{obs,max}$ is the maximum $\Delta\Delta G°_{obs}$ at high divalent ion concentration, [2+] is the molar concentration of either Mg^{2+} or putrescine^{2+}, $[2+]_0$ is the divalent ion concentration at the midpoint (half-maximal -$\Delta\Delta G°_{obs}$) of the curve, and *n* is the Hill exponent. Note this y-axis is free energy, instead of the more familiar fraction folded. The number of excess divalent ions taken up in the folding transition is given by the Wyman linkage relation

$$\Delta\Gamma_{2+} = -\left(\frac{1}{RT}\right)\left(\frac{\partial(\Delta\Delta G^0)}{\partial \ln[2+]}\right)_{T,P,[KCl]} \quad (5)$$

where R is the gas constant and T the temperature. The value of this derivative at the midpoint of the $\Delta\Delta G°_{obs}$ curve is related to the exponent *n* by

$$\Delta\Gamma_{2+} = n\left(\frac{-\Delta\Delta G^0_{\max}}{4RT}\right) \quad (6)$$

A similar equation is derived in ref. (15). We emphasize that $\Delta\Gamma_{2+}$ calculated from eq (6) applies only at the midpoint of the $\Delta\Delta G°_{obs}$ curve; $\Delta\Gamma_{2+}$ approaches zero at low and high divalent ion concentrations.

Results

RNA Selection

To survey the effects of putrescine on the stability of RNA tertiary structure, four RNAs that differ in their interactions with inorganic ions were selected for study (Figures 1 and S1). In this work, we distinguish “chelated” ions from all other cations interacting with an RNA, which we group together as the “ion atmosphere”. Chelated ions make at least two direct contacts with RNA electronegative groups, and are thus partially dehydrated; they are found in pockets of high negative electrostatic potential (16, 17). The ion atmosphere encompasses both fully hydrated ions at a distance from the RNA surface, and ions whose first-shell waters of hydration may be perturbed by the RNA surface (18).

The aptamer domain of the *add* adenine riboswitch (A-riboswitch, Figure S1A) was chosen as representative of a structured RNA exclusively stabilized by the ion atmosphere. The A-riboswitch folds into its native structure in the absence of divalent ions upon addition of adenine (or adenine derivatives) to the solution (19, 20). Although the RNA shows increased stability in the presence of Mg^{2+} (20, 21), crystallographic studies do not resolve any chelated Mg^{2+} or K^+ ions (22, 23). In addition, studies on the monovalent ion dependence of A-riboswitch concluded that this RNA shows no monovalent ion selectivity that might suggest K^+ chelation (9).

The homodimeric tetraloop receptor RNA (TLR RNA, Figure S1B) incorporates a motif first resolved in the *Tetrahymena* group I intron (24-26). This motif is known to chelate a K^+ ion (27), and is more stable in the presence of K^+ than other group I monovalent ions (9). When the TLR RNA dimerizes, two helical segments come into parallel alignment, a common arrangement in large RNAs. Because the negatively charged helices are brought fairly close together, there is a strong monovalent salt dependence to dimerization; however, Mg^{2+} is not essential for dimerization (9).

An rRNA fragment (58mer RNA, Figure S1C) and the aptamer domain of the M-box riboswitch (M-box RNA, Figure S1D) were chosen as examples of RNAs that chelate Mg^{2+}.

Structural studies of the 58mer RNA have concluded that both K^+ and Mg^{2+} are chelated in close proximity within the native fold of the 58mer (28, 29). This RNA obtains maximum stability in the presence of K^+ relative to other group I monovalent ions (30). In addition, electrostatic calculations concluded that a pocket of high negative potential on the RNA is capable of providing enough free energy to partially dehydrate and bind a Mg^{2+} ion (17). The M-box riboswitch is a sensor of the effective Mg^{2+} concentration *in vivo*(31). It is the largest of the RNAs used in this study (160 base pairs), and has a compact core that chelates at least three Mg^{2+} and three K^+ ions.

The two Mg^{2+}-chelating RNAs are distinct in their reliance on Mg^{2+} for folding to the native state. In the absence of a divalent ion, the 58mer requires 1.6 M NH_4Cl (32), and the M-box RNA does not fold even in 2.1 M NaCl (31). In the following sections, the two "Mg^{2+}- chelator" RNAs will be discussed separately from the other two RNAs, which fold to their native structures in modest concentrations of KCl.

Comparison of A-riboswitch and TLR RNA stabilities with putrescine^{2+} vs. Mg^{2+}

RNA stabilities were assessed using thermal melts monitored by UV absorbance (see Materials & Methods). Conditions are readily found under which both the A-riboswitch and TLR RNA fold to their native structures in the absence of divalent ions. The A-riboswitch folds in the presence of a tight-binding ligand (20 μM 2,6-diaminopurine, DAP) and 50 mM K^+; a higher monovalent salt concentration (300 mM K^+) is needed to observe the TLR RNA dimer. For the A-riboswitch, a distinctive unfolding transition is only observed in the presence of ligand and corresponds to the loss of tertiary structure (20). The transition shifts to higher T_m upon addition of either putrescine^{2+} or Mg^{2+} (Figure S2A). Dimerization of the TLR RNA is accompanied by a small but distinctive transition that is slightly hyperchromic at 260 nm and hypochromic at 280 nm; its T_m is also concentration-dependent as expected for a dimerization reaction (9). This transition also shifts to higher temperature in response to either Mg^{2+} or putrescine^{2+} (Figure S2B, S2C). Melting curves obtained under these buffer conditions can thus be analyzed to obtain standard free energies for tertiary structure folding, ΔG°_{obs}, in the presence or absence of divalent ion (see Materials and Methods).

Figure 2 plots the increment in folding free energy due to the divalent ion:

$$\Delta\Delta G^\circ_{obs} = \Delta G^\circ_{obs,2+} - \Delta G^\circ_{obs,ref} \quad (1)$$

where $\Delta G^\circ_{obs,ref}$ is the folding free energy in the reference buffer with only monovalent ions, and $\Delta G^\circ_{obs,2+}$ the folding free energy with a given concentration of divalent ion. There is a striking difference in the effectiveness of the two ions; it takes 6 – 8 fold higher putrescine^{2+} concentration to achieve the same stability increase as with Mg^{2+}.

To contrast the effectiveness of the two different ions in thermodynamic terms, the comparison should be made between RNA stabilities at the same ion activities, rather than ion concentrations. The activity of $MgCl_2$ over a range of concentrations is known (11, 33), and the mean ionic activity coefficient of millilmolar concentrations of Mg^{2+} in the presence of 50 mM KCl can be estimated as ~0.66 (10). To our knowledge, there are no similar measurements of putrescine•2HCl activity. We carried out vapor pressure osmometry experiments to address this question (see Materials and Methods, Figure S4). Although it is difficult to measure putrescine osmolalities at low concentrations accurately, we argue from the data that $MgCl_2$ and putrescine•2HCl differ in activity by much less than a factor of two at the concentrations used in our experiments. We conclude that a difference in thermodynamic activity of Mg^{2+} and putrescine^{2+} cannot account for the large difference in concentrations needed to stabilize these two RNAs, and that it is reasonable to use a

concentration scale when comparing RNA folding free energies measured with these two ions.

Besides the difference in the ability of the two divalent ions to stabilize RNA, another interesting feature of Figure 2 is the difference in uptake of divalent ion that accompanies the folding reaction. We express the number of "excess" divalent ions per RNA that are present in order to neutralize part of the RNA negative charge as Γ_{Mg2+} (for Mg^{2+}) or Γ_{put2+} (for putrescine^{2+}). Upon folding from a partially structured RNA to a more compact native conformation, Γ_{2+} invariably increases (20, 34). Under the conditions of excess K^+ employed here, $\Delta\Gamma_{2+}$ evaluated at the divalent ion concentration required to fold half of the RNA molecules is identical to the Hill exponent *n* obtained by fitting the Hill equation to a plot of fraction RNA folded vs. ln[Mg^{2+}] (20). In Figure 2, the slope $d(\Delta\Delta G°_{obs})/d(\ln[Mg^{2+}]$, evaluated at the midpoint of the $\Delta\Delta G°_{obs}$ curve, is related to the same parameter (see Materials and Methods, eq 5). For both RNAs, $\Delta\Gamma_{Mg2+}$ is larger than $\Delta\Gamma_{put2+}$, though the large error in $\Delta\Gamma_{put2+}$ for the TLR RNA means the difference is less significant. (The error is from uncertainty in the maximum value of -ΔΔG°obs; data cannot be collected at higher putrescine concentrations without biasing the measurement with a large excess of Cl^- ions (20).) $\Delta\Gamma_{2+}$ is not independent of divalent ion concentration, so a comparison between $\Delta\Gamma_{Mg2+}$ and $\Delta\Gamma_{put2+}$ could be misleading because of the large difference in ion concentrations at the midpoints of the two curves. The expectation is that $\Delta\Gamma_{2+}$ increases with the divalent ion concentration (20), but we find that the ion at higher concentration, putrescine^{2+}, has the smaller value of $\Delta\Gamma_{2+}$. The difference in ion uptake therefore appears to be a real difference in the behaviors of the ions.

Finally, it appears that putrescine^{2+} does not stabilize either the A-riboswitch or TLR RNA to the same $\Delta\Delta G°_{obs,max}$ as Mg^{2+}. As noted above, there is a large uncertainty in the maximum stability of the TLR RNA with putrescine^{2+}, but the difference in the A-riboswitch stabilities with the two ions is significant (-1.06 ± 0.20 kcal/mol, see Table 1). Since $\Delta\Gamma_{Mg2+}$ and $\Delta\Gamma_{put2+}$ are different for this RNA, it is not surprising that $\Delta\Delta G°_{obs,max}$ is also different. Whether the difference stems from a stronger interaction of Mg^{2+} with the native state, a stronger interaction of putrescine^{2+} with partially unfolded RNA conformations, or both those factors, cannot be decided from the present experiments. Ideas about the relation between charge density of ions and their interactions with RNA are taken up in the Discussion.

A-riboswitch stability with various diamines

To better understand how putrescine^{2+} interacts with RNA, several diamines with different carbon linkers were used to ask whether RNA stability depends on either the average distance between amines or the rigidity of the linker. $\Delta\Gamma_{put2+}$ weakly varies between ~2.2 and 2.4 with different diamines, and is largest with the shortest alkyl linker (Table 1). The midpoint of the titration curve varies more significantly, by about a factor of three (Figure 3A). To ask whether stabilization free energy imparted by a given diamine is correlated with the average intramolecular distance between amine groups in solution, the first acid dissociation constant (pK_a) for each diamine was obtained (Table 1). Deprotonation of an amine is energetically less costly if a second positive charge is nearby. Based on Coulomb's law, the first pK_a is inversely proportional to the distance between the two charges. A plot of $\Delta\Delta G°_{obs}$ at a specific diamine concentration (2 mM) vs. the first pK_a of the cation results in an approximately linear trend (Figure 3B).

A-riboswitch and TLR RNA stability in mixed Mg^{2+} - putrescine buffers

As shown in Figure 2, Mg^{2+} stabilizes the A-riboswitch and TLR RNA more effectively than putrescine^{2+}. Under *in vivo* conditions, though, RNA is stabilized by a mixture of

several different counter ions. In order to assess how mixtures of putrescine^{2+} and Mg^{2+} influence the stability of RNA, we conducted thermal melts on our set of four RNAs with varying concentrations of the two divalent ions. To help interpret the results, we note that an excess of cations and an exclusion of anions balance the charge of anionic phosphates on the RNA, as required by charge neutrality. Thus, any change in $\Delta\Gamma_{put2+}$ (for instance) must be compensated by a change in the excess of other ionic species in solution (15, 34):

$$-2\Delta\Gamma_{put2+}=2\Delta\Gamma_{Mg^{2+}}+\Delta\Gamma_{K+}-\Delta\Gamma_{Cl-} \quad (2)$$

Figure 4A shows the change in A-riboswitch stability vs. concentration of putrescine^{2+}, with the Mg^{2+} concentration kept constant at the indicated values. The negative slopes of these curves indicate a net uptake of putrescine^{2+} ions upon folding the RNA to its native state (see Materials and Methods, eq 5). As the Mg^{2+} concentration increases from 0. 1mM to 0.5 mM the resulting change in free energy upon addition of putrescine^{2+} becomes less negative, though the maximum uptake ($\Delta\Gamma_{put2+} \approx 1.4$ ions/RNA at 2 mM putrescine^{2+} and 0.1 mM Mg^{2+}, Figure 4A) and $-\Delta\Delta G°_{obs}$ at a given putrescine^{2+} concentration are never as great as seen with putrescine^{2+} alone (Figure 2). Thus, the uptake of putrescine^{2+} is opposed by increased Mg^{2+} concentrations, as might be expected on the basis of eq (2). The release of Mg^{2+} can be estimated from the dependence of $\Delta\Delta G°_{obs}$ on Mg^{2+} concentration at a constant putrescine^{2+} concentration (eq 1). At 2 mM putrescine and 0.1 mM Mg^{2+}, $\Delta\Gamma_{2+} \approx$ -1.4 (Figure 4A). Although it appears that $\Delta\Gamma_{Mg2+}$ and $\Delta\Gamma_{put2+}$ are equal and opposite, these estimates are not accurate enough to rule out small accompanying changes in $\Delta\Gamma_{K+}$ and $\Delta\Gamma_{Cl-}$.

The TLR RNA also shows a net stabilization upon addition of putrescine^{2+} to a Mg^{2+}-containing buffer (Figure 4B). The trend in $\Delta\Delta G°_{obs}$ is qualitatively similar to the A-riboswitch, although the magnitude of the stabilization is about twice as large for the TLR RNA. (In 0.2 mM $MgCl_2$ and 10 mM putrescine^{2+}, the TLR RNA obtains a maximum stability of -4.03 kcal/mol ± 0.19 kcal/mol, versus −2.03 kcal/mol ± 0.12 kcal/mol for the A-riboswitch.)

Stability of Mg^{2+} -chelator RNAs in mixed Mg^{2+} - putrescine buffers

Melting curves of both Mg^{2+}-chelator RNAs show the appearance of a new transition with a distinctive ratio of hyperchromicities at 260 and 280 nm when ~1 mM $MgCl_2$ is included in the buffer, in addition to 50-60 mM KCl (35) (Figure 5 and S3 D-F). This transition is not observed when putrescine^{2+} is substituted for Mg^{2+} at concentrations up to 10 mM; apparently putrescine^{2+} cannot provide enough free energy of stabilization at the accessible concentrations. When the two Mg^{2+}-chelating RNAs are first induced to fold by Mg^{2+} and then titrated with putrescine^{2+}, the stability decreases (Figure 6 A, B). The 58mer RNA is destabilized only by putrescine^{2+} concentrations in excess of ~2 mM (0.5 to 2.0 mM $MgCl_2$), but the M-box riboswitch is destabilized by >1.8 kcal/mol at 2 mM putrescine^{2+} and ≤ 1 mM Mg^{2+}. Tertiary structure is undetectable in either RNA at a high enough ratio of putrescine^{2+} to Mg^{2+} ions. This behavior is the opposite from our observations with the A-riboswitch and TLR RNA in mixed Mg^{2+} - putrescine^{2+} buffers (Figure 4).

Discussion

In vivo relevance of putrescine to RNA folding

In vivo, the stability of an RNA structure may be affected by several different solution components, such as ions, osmolytes (36), and other macromolecules that act as crowding agents (37). Of the three most abundant cations in the bacterial cell, K^+, Mg^{2+} and

putrescine^{2+}, relatively little is known about the effects of putrescine^{2+} on RNA stability. In this work, we try to gain some insight into the *in vivo* relevance of putrescine^{2+} to RNA folding by asking what change the ion causes in folding free energy ($\Delta\Delta G°_{obs}$) and what degree of ion uptake is associated with structure formation ($\Delta\Gamma_{put2+}$) for four different RNA tertiary structures.

The experiments reported here show that putrescine^{2+} is, in general, far less effective than Mg^{2+} at stabilizing RNA tertiary structure: two of the RNAs required more than five-fold higher concentrations of putrescine^{2+} than Mg^{2+} to reach the same stability (Figure 3), and two RNAs could not be induced to fold to the native structure in buffers with only putrescine^{2+} and monovalent ions. Putrescine^{2+} has also been found to be a very weak stabilizer of tRNA tertiary structure, compared to Mg^{2+} (4). The question of whether these weak effects may influence RNA stability *in vivo* is difficult to answer definitively. We first consider the range of ion activities that are likely to be found in bacteria *in vivo*, and then discuss the potential consequences for RNA tertiary folding.

The *in vivo* activity of Mg^{2+} is difficult to measure, but several kinds of measurements suggest it is equivalent to that of ~1.0 mM Mg^{2+} in the presence of 150 mM KCl, (38-40). (The total cellular concentration of Mg^{2+} is about 100 fold higher (2), but because the ion interacts so strongly with cellular polynucleotides the effective concentration, or activity, is much lower.) The measurements in the present work were made in a background of 50 to 300 mM K^+, with most of the anion as Cl^-. At 50 mM KCl, the concentration of Mg^{2+} needed to reproduce the estimated *in vivo* activity is ~0.30 mM. (This calculation is based on $MgCl_2$ and KCl activity coefficients and the principle that the mean ionic activity coefficient of a low concentration of Mg^{2+} in 50 mM KCl is the same as the mean ionic activity coefficient of Mg^{2+} in a $MgCl_2$ solution of the same ionic strength as 50 mM KCl, i.e. 17 mM $MgCl_2$(10).) These are rough estimates, but nevertheless, the four RNAs studied here are all significantly stabilized by submillimolar Mg^{2+} concentrations that are probably comparable to *in vivo* activities. The M-box RNA is in fact a regulatory switch that turns on or off expression of a Mg^{2+} transporter gene in response to changes in Mg^{2+} concentration *in vivo*, so this RNA might be expected to fold or unfold near physiological Mg^{2+} activity (31, 41).

We are not aware of any estimates of *in vivo* putrescine^{2+} activity. If we take the *in vivo* total concentration under standard growth conditions to be 60 mM (1), and the same ~100:1 ratio of total to effective concentration as Mg^{2+}, the activity would be the equivalent of ~0.2 mM putrescine^{2+} in 50 mM KCl (or 0.6 mM at 150 mM KCl). However, the apparent affinity of putrescine^{2+} for helical DNA is 2-3 fold weaker than that of Mg^{2+} (3), and interactions with RNA may be even weaker, as suggested by the experiments reported here. The ratio of total to effective concentration may therefore be much smaller than 100:1, and the effective concentration *in vivo* somewhat higher than that of Mg^{2+}. We consider 0.2 –1.0 mM putrescine^{2+} (50 mM KCl) a reasonable range for reproducing *in vivo* conditions.

Given the above considerations, it seems likely that, in the context of the bacterial cell, putrescine^{2+} makes a small but significant contribution to the overall stability of an RNA. For instance, 0.2 to 1.0 mM putrescine^{2+} stabilizes the A-riboswitch by -1.4 to -3.3 kcal/mol. Though these values drop by a factor of five in the presence of 0.2 mM Mg^{2+}, even a –0.5 kcal/mol free energy gain over Mg^{2+} alone is enough to shift a folding equilibrium. The M-box RNA is a particularly interesting case, in which putrescine^{2+} *destabilizes* the RNA by nearly 2 kcal/mol when present at only twice the Mg^{2+} concentration (Figure 6B). For a sensor RNA that is tuned to respond to intracellular fluctuations in Mg^{2+} activity, this free energy change is quite significant. Noting that putrescine^{2+} concentrations may vary over at least an eight fold range as the osmolality of the growth medium changes (1), there is the

intriguing possibility that the responses of the M-box RNA or other riboswitches are modulated to some extent by intracellular putrescine^{2+} activity.

A caveat about the distribution of putrescine in nature is necessary. Microorganisms such as bacteria and molds contain high concentrations of putrescine^{2+} (42), and *E. coli* requires polyamines for growth under anaerobic conditions (43). However, mammalian cells cells typically contain putrescine^{2+} in approximately 2-3 orders of magnitude lower concentration (42), which are unlikely to affect the folding or stability of any RNAs. The two riboswitches selected for this study are found exclusively in bacteria; consequently their structures may have evolved in response to the high bacterial levels of putrescine. The other two RNAs represent a motif and a structure that are found in all organisms, but it is still possible that their stability is modulated by putrescine in bacteria, and that the specific sequences utilized by the organism or other factors (such as a bound protein, (44)) compensate.

RNA stabilization by divalent ions of the "ion atmosphere"

A question raised by this and other studies of putrescine^{2+} with RNA (4, 5) is why putrescine^{2+} is less effective at stabilizing RNA, in comparison to Mg^{2+}; this study additionally poses the question of why putrescine^{2+} destabilizes some RNAs when Mg^{2+} is present. For the purposes of the following discussion, it is convenient to use the distinction (see Results) between *chelated* ions that directly contact two or more RNA groups, and the *ion atmosphere*, defined here as the remaining cations that interact with an RNA at various distances from the RNA surface. Putrescine^{2+}, or any other cation, is capable of favorable interaction with the RNA as a part of the ion atmosphere, but putrescine^{2+} is very unlikely to substitute for an inorganic ion at a chelation site. (We know of no RNA that specifically binds putrescine^{2+} in a way analogous to the chelation of an inorganic ion, though recognition of the amino-butyl side chain of lysine by the lysine riboswitch suggests such a site is feasible (45, 46).) We consider the ion atmosphere first and then discuss the possible effects of putrescine^{2+} on Mg^{2+} chelation sites.

Ion atmosphere—The A-riboswitch and TLR RNAs were selected as examples of RNAs for which Mg^{2+}-induced stabilization is entirely by RNA interactions with the ion atmosphere; as detailed in Results, there is no evidence for Mg^{2+} chelation sites in either RNA. Our conclusions for these two RNAs are that (i) Mg^{2+} is always more stabilizing than putrescine^{2+} (Figure 2); (ii) $\Delta\Gamma_{2+}$ is perhaps slightly less for putrescine^{2+} than for Mg^{2+}; and (iii) the stabilizing effect of Mg^{2+} and putrescine^{2+} together, while not additive, is always as least as strong as that of either of the ions alone (cf. Figures 2 and 4). Thus, with respect to the ion atmosphere, putrescine^{2+} apparently substitutes to some extent for Mg^{2+}, but is not as effective. An argument has been made that ions with higher charge density (defined as charge divided by Van der Waals volume) are more effective stabilizers of native RNA structures because they may approach the RNA surface (and maximum negative electrostatic potential) more closely, and because of smaller excluded volume effects when ions accumulate in high concentration near the RNA (5). Our results with Mg^{2+} and putrescine^{2+} are consistent with this idea.

To further explore the way charge density might affect the interactions of organic ions with RNA, we compared the stability of the A-riboswitch with five different organic diamino compounds. The results (Figure 3 and Table 1) show distinct dependences on the length and saturation of the carbon chain separating the two charges. The first pK_a of these ions varies over a range of ~1.5 pH units; it is a measure of the reciprocal distance between the two charges. To a good approximation, the stabilization imparted by the ion is proportional to a *linear* charge density, *i.e.* the charge divided by the average distance of separation (Figure 3B). However, an additional factor to consider is that the linear charge density of an organic

ion may be influenced by its environment. In the diamino alkane compounds, the average distance of separation between two amino groups could decrease as the ion approaches the RNA surface, if the decrease in entropy is sufficiently compensated by the simultaneous placement of the two amines in a volume of high negative electrostatic potential. In fact, 1,4 *trans*-diaminobutene, which is locked in a more extended conformation than either putrescine or 1,4 *cis*-diaminobutene, imparts 0.45 kcal/mol less negative $\Delta\Delta G°_{obs}$ than expected based on the correlation between pK_a and $\Delta\Delta G°_{obs}$ for the diamino-alkanes. Thus, both the flexibility and length of carbon chains may be factors in determining how effectively organic ions (including spermine and spermidine) interact with compact RNAs.

Chelation sites—RNAs that contain Mg^{2+} chelation sites tend to be strongly dependent on Mg^{2+} to fold into their native structures, presumably because it is too costly to create the high electrostatic potential of an ion binding pocket if there is no cation capable of occupying the site (17, 47, 48). Steric constraints prevent putrescine^{2+} from replacing Mg^{2+} in a chelation site, so it is unsurprising that putrescine^{2+} (plus monovalent cation) are unable to stabilize the native state of either the 58mer or M-box RNAs. It is less obvious why addition of putrescine^{2+} should destabilize an RNA that has been driven into its native conformation by Mg^{2+} (Figure 6). The observation suggests that putrescine^{2+} weakens the affinity of Mg^{2+} for chelation sites, but there cannot be direct competition between the ions for occupancy of the site. To rationalize this observation, we turn to a calculation of the repulsive interactions between chelated Mg^{2+} and the ion atmosphere (17, 48). Occupancy of a chelation site by Mg^{2+} effectively neutralizes two negative charges of the RNA backbone and results, at high enough Mg^{2+} concentration, in the displacement of an approximately equivalent positive charge from among the divalent cations of the ion atmosphere. This displacement of favorably-interacting cations is an apparent repulsive (positive free energy) between site-bound Mg^{2+} and the ion atmosphere. As Mg^{2+} is titrated, the actual free energy (rather than the standard state free energy) of Mg^{2+}-RNA interactions at the chelated site and in the ion atmosphere change in different ways (cf. Figure 2 of ref. (48)):

- The free energy of site-bound Mg^{2+}, ΔG_{site}, decreases linearly (becomes more negative) with the logarithm of the Mg^{2+} activity;
- The repulsive interaction between the site-bound ion and the ion atmosphere, $\Delta G_{IA\text{-}S}$, increases continuously with log[Mg^{2+}].

For 1 mM Mg^{2+} interacting with the 58mer RNA (60 mM KCl), ΔG_{site} is estimated from experiments to be −4.5 kcal/mol, which is far larger than the calculated repulsive term (+1.2 kcal/mol under the same conditions (48)). We suggest that the contribution of putrescine^{2+} to a site-binding term must be nearly zero, as the ion cannot effectively take advantage of the small chelation site. However the second, repulsive term between Mg^{2+} in the chelation site and putrescine^{2+} in the ion atmosphere will persist and increase with increasing putrescine^{2+} concentration. It is this “repulsive” free energy that could reduce the free energy gain from Mg^{2+} chelation and cause a net destabilization of the RNA at high putrescine^{2+} concentrations.

Putrescine^{2+} vs. Mg^{2+} in vivo

In summary, in comparison to Mg^{2+}, putrescine^{2+} is most likely a minor contributor to the overall stability of an RNA tertiary structure *in vivo*. However, putrescine^{2+} has the curious property of being able to tip the thermodynamic scales towards either folded or unfolded forms of an RNA, depending on the architecture of the specific RNA. This observation leads us to hypothesize that the evolution of functional RNA structures has been influenced by the presence of putrescine^{2+} in the cellular ionic environment.

Supplementary Material

Refer to Web version on PubMed Central for supplementary material.

Acknowledgments

We thank members of the Townsend lab for help in synthesizing both *cis* and *trans*-1,4-diaminobutene, and Ryan Hulscher and Andrew Buller for helpful comments on the manuscript.

This work was supported by NIH grants RO1 GM58545 and T32 GM008403 (Program in Molecular Biophysics), and the Francis D. Carlson Fellowship (to RJT).

References

1. Capp MW, Cayley DS, Zhang W, Guttman HJ, Melcher SE, Saecker RM, Anderson CF, Record MT Jr. Compensating effects of opposing changes in putrescine (2+) and K+ concentrations on lac repressor-lac operator binding: in vitro thermodynamic analysis and in vivo relevance. J Mol Biol. 1996; 258:25–36. [PubMed: 8613989]
2. Kuhn A, Kellenberger E. Productive phage infection in Escherichia coli with reduced internal levels of the major cations. J Bacteriol. 1985; 163:906–912. [PubMed: 3161872]
3. Braunlin WH, Strick TJ, Record MT Jr. Equilibrium dialysis studies of polyamine binding to DNA. Biopolymers. 1982; 21:1301–1314. [PubMed: 7115891]
4. Heerschap A, Walters JALI, Hilbers CW. Interactions of some naturally occurring cations with phenylalanine and initiator tRNA from yeast as reflected by their thermal stability. Biophys Chem. 1985; 22:205–217. [PubMed: 3902111]
5. Koculi E, Hyeon C, Thirumalai D, Woodson SA. Charge Density of Divalent Metal Cations Determines RNA Stability. J Am Chem Soc. 2007; 129:2676–2682. [PubMed: 17295487]
6. Grilley D, Soto AM, Draper DE. Direct quantitation of Mg2+-RNA interactions by use of a fluorescent dye. Methods Enzymol. 2009; 455:71–94. [PubMed: 19289203]
7. Martin B, Posseme F, Le Barbier C, Carreaux F, Carboni B, Seiler N, Moulinoux JP, Delcros JG. (Z)-1,4-diamino-2-butene as a vector of boron, fluorine, or iodine for cancer therapy and imaging: synthesis and biological evaluation. Bioorg Med Chem. 2002; 10:2863–2871. [PubMed: 12110306]
8. He B, Rong M, Lyakhov D, Gartenstein H, Diaz G, Castagna R, McAllister WT, Durbin RK. Rapid mutagenesis and purification of phage RNA polymerases. Protein Expr Purif. 1997; 9:142–151. [PubMed: 9116496]
9. Lambert D, Leipply D, Shiman R, Draper DE. The influence of monovalent cation size on the stability of RNA tertiary structures. J Mol Biol. 2009; 390:791–804. [PubMed: 19427322]
10. Harned, HS.; Robinson, RA. Multicomponent Electrolyte Solutions. Vol. 15. Pergamon Press; Oxford: 1968.
11. Kumbhar RR, Dagade DH, Terdale SS, Patil KJ. Thermodynamic Equilibrium Constant Studies on Aqueous Electrolytic (Alkaline Earth Chlorides) Solutions Containing 18-Crown-6 at 298.15K. J Solution Chem. 2007; 36:259–273.
12. Levine, IN. Physical Chemistry. 5th. McGraw Hill; 2002.
13. Robinson, RA.; Stokes, RH. Electrolyte Solutions. Second Revised. Dover Publications; Minoeola, NY: 2002.
14. Draper, DE.; Bukhman, YV.; Gluick, TC. Thermal Methods for the Analysis of RNA Folding Pathways. In: Beaucage, SL.; Bergstrom, DE.; Glick, GD.; Jones, RA., editors. Current Protocols in Nucleic Acid Chemistry. Vol. section 11.13. John Wiley & Sons; New York: 2000. p. 13
15. Leipply D, Lambert D, Draper DE. Ion-RNA interactions thermodynamic analysis of the effects of mono- and divalent ions on RNA conformational equilibria. Methods Enzymol. 2009; 469:433–463. [PubMed: 20946802]
16. Cate JH, Hanna RL, Doudna JA. A magnesium ion core at the heart of a ribozyme domain. Nat Struct Biol. 1997; 4:553–558. [PubMed: 9228948]
17. Misra VK, Draper DE. A thermodynamic framework for Mg^{2+} binding to RNA. Proc Natl Acad Sci U S A. 2001; 98:12456–12461. [PubMed: 11675490]

18. Draper DE, Grilley D, Soto AM. Ions and RNA folding. Annu Rev Biophys Biomol Struct. 2005; 34:221–243. [PubMed: 15869389]
19. Noeske J, Schwalbe H, Wohnert J. Metal-ion binding and metal-ion induced folding of the adenine-sensing riboswitch aptamer domain. Nucleic Acids Res. 2007; 35:5262–5273. [PubMed: 17686787]
20. Leipply D, Draper DE. Dependence of RNA tertiary structural stability on Mg2+ concentration: interpretation of the Hill equation and coefficient. Biochemistry. 2010; 49:1843–1853. [PubMed: 20112919]
21. Lemay JF, Penedo JC, Tremblay R, Lilley DM, Lafontaine DA. Folding of the adenine riboswitch. Chem Biol. 2006; 13:857–868. [PubMed: 16931335]
22. Batey RT, Gilbert SD, Montange RK. Structure of a natural guanine-responsive riboswitch complexed with the metabolite hypoxanthine. Nature. 2004; 432:411–415. [PubMed: 15549109]
23. Serganov A, Yuan YR, Pikovskaya O, Polonskaia A, Malinina L, Phan AT, Hobartner C, Micura R, Breaker RR, Patel DJ. Structural basis for discriminative regulation of gene expression by adenine- and guanine-sensing mRNAs. Chem Biol. 2004; 11:1729–1741. [PubMed: 15610857]
24. Jaeger L, Westhof E, Leontis NB. TectoRNA: modular assembly units for the construction of RNA nano-objects. Nucleic Acids Res. 2001; 29:455–463. [PubMed: 11139616]
25. Davis JH, Tonelli M, Scott LG, Jaeger L, Williamson JR, Butcher SE. RNA helical packing in solution: NMR structure of a 30 kDa GAAA tetraloop-receptor complex. J Mol Biol. 2005; 351:371–382. [PubMed: 16002091]
26. Zuo X, Wang J, Foster TR, Schwieters CD, Tiede DM, Butcher SE, Wang YX. Global molecular structure and interfaces: refining an RNA:RNA complex structure using solution X-ray scattering data. J Am Chem Soc. 2008; 130:3292–3293. [PubMed: 18302388]
27. Basu S, Rambo RP, Strauss-Soukup J, Cate JH, Ferré-D'Amare AR, Strobel SA, Doudna JA. A Specific Monovalent Metal Ion Integral to the A-A Platform of the RNA Tetraloop Receptor. Nature Struc Biol. 1998; 5:986–992.
28. Conn GL, Draper DE, Lattman EE, Gittis AG. Crystal structure of a conserved ribosomal protein-RNA complex. Science. 1999; 284:1171–1174. [PubMed: 10325228]
29. Conn GL, Gittis AG, Lattman EE, Misra VK, Draper DE. A compact RNA tertiary structure contains a buried backbone-K^+ complex. J Mol Biol. 2002; 318:963–973. [PubMed: 12054794]
30. Shiman R, Draper DE. Stabilization of RNA tertiary structure by monovalent cations. J Mol Biol. 2000; 302:79–91. [PubMed: 10964562]
31. Dann CE 3rd, Wakeman CA, Sieling CL, Baker SC, Irnov I, Winkler WC. Structure and mechanism of a metal-sensing regulatory RNA. Cell. 2007; 130:878–892. [PubMed: 17803910]
32. Bukhman YV, Draper DE. Affinities and Selectivities of Divalent Cation Binding Sites Within an RNA Tertiary Structure. J Mol Biol. 1997; 273:1020–1031. [PubMed: 9367788]
33. Robinson, RA.; Stokes, RH. Electrolyte Solutions. 2nd. Butterworth & Co. Ltd; London: 1970.
34. Grilley D, Soto AM, Draper DE. Mg2+-RNA interaction free energies and their relationship to the folding of RNA tertiary structures. Proc Natl Acad Sci U S A. 2006; 103:14003–14008. [PubMed: 16966612]
35. Lu M, Draper DE. Bases defining an ammonium and magnesium ion-dependent tertiary structure within the large subunit ribosomal RNA. J Mol Biol. 1994; 244:572–585. [PubMed: 7527467]
36. Lambert D, Draper DE. Effects of Osmolytes on RNA Secondary and Tertiary Structure Stabilities and RNA-Mg^{2+} Interactions. J Mol Biol. 2007; 370:993–1005. [PubMed: 17555763]
37. Kilburn D, Roh JH, Guo L, Briber RM, Woodson SA. Molecular crowding stabilizes folded RNA structure by the excluded volume effect. J Am Chem Soc. 2010; 132:8690–8696. [PubMed: 20521820]
38. Froschauer EM, Kolisek M, Dieterich F, Schweigel M, Schweyen RJ. Fluorescence measurements of free [Mg2+] by use of mag-fura 2 in Salmonella enterica. FEMS Microbiol Lett. 2004; 237:49–55. [PubMed: 15268937]
39. London RE. Methods for measurement of intracellular magnesium: NMR and fluorescence. Annu Rev Physiol. 1991; 53:241–258. [PubMed: 2042961]

40. Alatossava T, Jutte H, Kuhn A, Kellenberger E. Manipulation of intracellular magnesium content in polymyxin B nonapeptide-sensitized Escherichia coli by ionophore A23187. J Bacteriol. 1985; 162:413–419. [PubMed: 2984182]
41. Cromie MJ, Shi Y, Latifi T, Groisman EA. An RNA sensor for intracellular Mg(2+). Cell. 2006; 125:71–84. [PubMed: 16615891]
42. Tabor CW, Tabor H. 1,4-Diaminobutane (putrescine), spermidine, and spermine. Annu Rev Biochem. 1976; 45:285–306. [PubMed: 786151]
43. Chattopadhyay MK, Tabor CW, Tabor H. Polyamines are not required for aerobic growth of Escherichia coli: preparation of a strain with deletions in all of the genes for polyamine biosynthesis. J Bacteriol. 2009; 191:5549–5552. [PubMed: 19542271]
44. Maeder C, Conn GL, Draper DE. Optimization of a ribosomal structural domain by natural selection. Biochemistry. 2006; 45:6635–6643. [PubMed: 16716074]
45. Garst AD, Heroux A, Rambo RP, Batey RT. Crystal structure of the lysine riboswitch regulatory mRNA element. J Biol Chem. 2008; 283:22347–22351. [PubMed: 18593706]
46. Serganov A, Huang L, Patel DJ. Structural insights into amino acid binding and gene control by a lysine riboswitch. Nature. 2008; 455:1263–1267. [PubMed: 18784651]
47. Das R, Travers KJ, Bai Y, Herschlag D. Determining the Mg2+ stoichiometry for folding an RNA metal ion core. J Am Chem Soc. 2005; 127:8272–8273. [PubMed: 15941246]
48. Leipply D, Draper DE. Evidence for a thermodynamically distinct Mg(2+) ion associated with formation of an RNA tertiary structure. J Am Chem Soc. 2011; 133:13397–13405. [PubMed: 21776997]
49. Sober, HA. CRC Handbook of Biochemistry. CRC Press; Cleveland, OH: 1968.
50. Dawson, RM.; Elliot, DC.; Elliot, WH.; Jones, KM. Data for Biochemical Research. Oxford Sciences Publications; Oxford: 1986.
51. Perrin, DD. Dissociation Constants of Organic Bases in Aqueous Solution (Supplement). Butterworths; London: 1972.

Abbreviation

DAP 2,6 diamino-purine

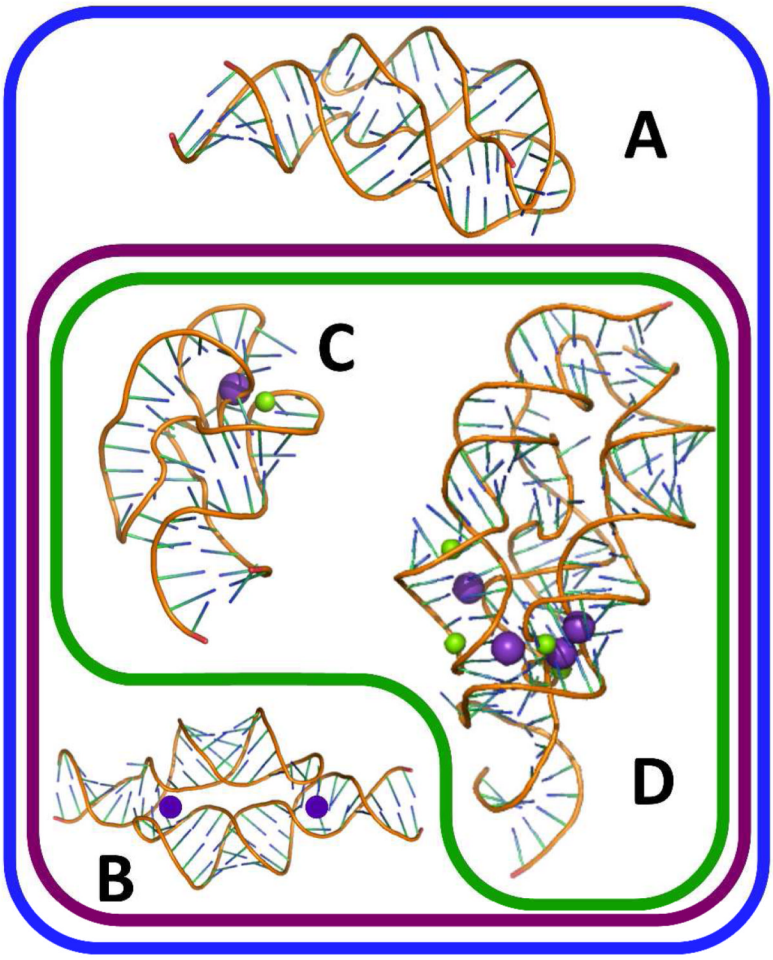

Figure 1.

Venn diagram depicting the RNA structures analyzed in this study and how they interact with cations. Blue outline contains population of RNAs stabilized by cations residing in the ion atmosphere. Purple outline contains RNAs that, in addition, have chelated K^+ ions (purple spheres). RNAs within the green outline also have chelated Mg^{2+} ions (green spheres). A) A-riboswitch, PDB ID: 3G4M. B) TLR RNA, PDB ID:2I7E; (K^+ ions have been added as discussed in text). C) 58mer rRNA, PDB ID: 1HC8. D) M-box riboswitch, PDB ID: 2QBZ. See Figure S1 for sequences used in this study.

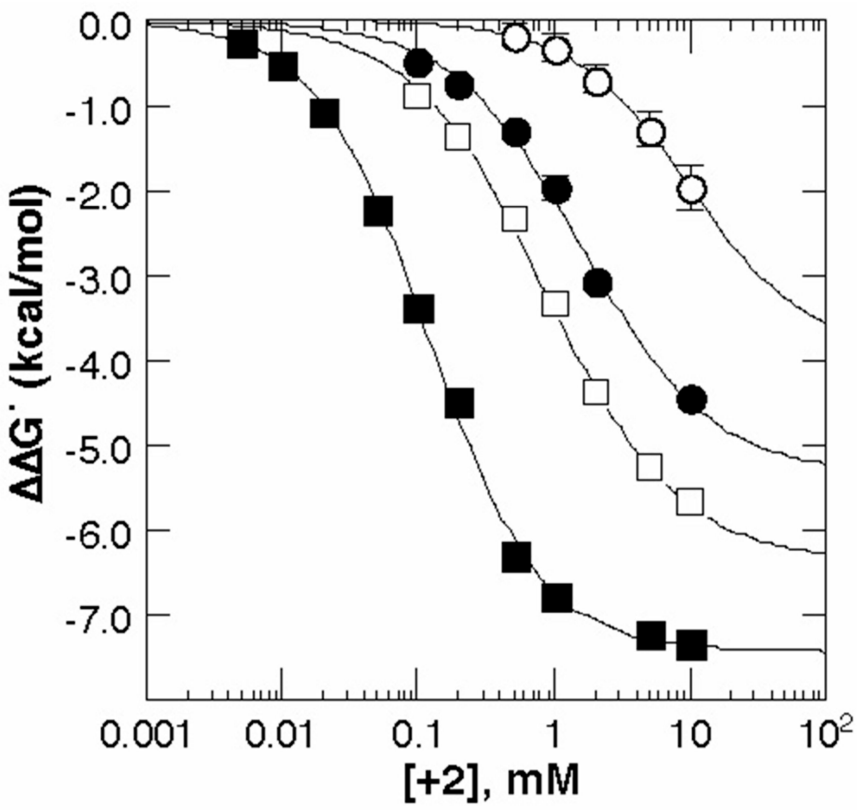

Figure 2.

The increase in stability ($\Delta\Delta G°_{obs}$, eq 1) upon titration of A-riboswitch (squares) or TLR RNA (circles) with chloride salts of Mg^{2+} (closed) or putrescine^{2+} (open). Tetraloop receptor data were collected in K•MOPS - EDTA buffer (see Materials and Methods) with 300 mM K^+ while the A-riboswitch data were collected in the same buffer with 50 mM K^+ and 20 μM DAP. Either $MgCl_2$ or putrescine•2HCl was added to the concentration indicated by the abscissa, [2+].

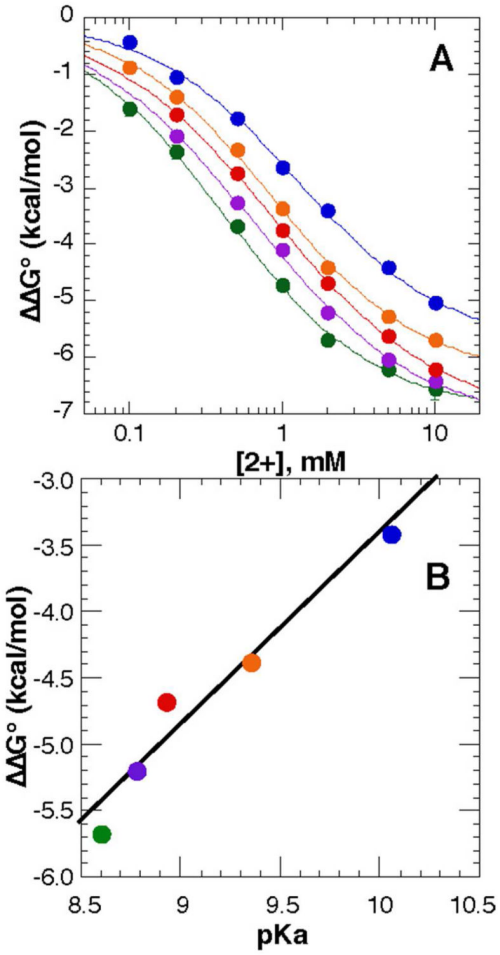

Figure 3.

Stability of the A-riboswitch in the presence of various diamines, as derived from thermal stability measurements. **A**, $\Delta\Delta G°_{obs}$ of the A-riboswitch vs. concentration of cadaverine (blue), putrescine (orange), trans-1,4-diaminobutene (red), cis-1,4-diaminobutene (purple) and 1,3-diaminopropane (green). **B**, stability of the A-riboswitch at 2 mM concentration of the diamines listed above vs the first acid dissociation constant (pK_a, Table 1) of the diamine. The slope of the least squares fit to all the data points (black line) is 1.45 kcal/mol (R=0.975).

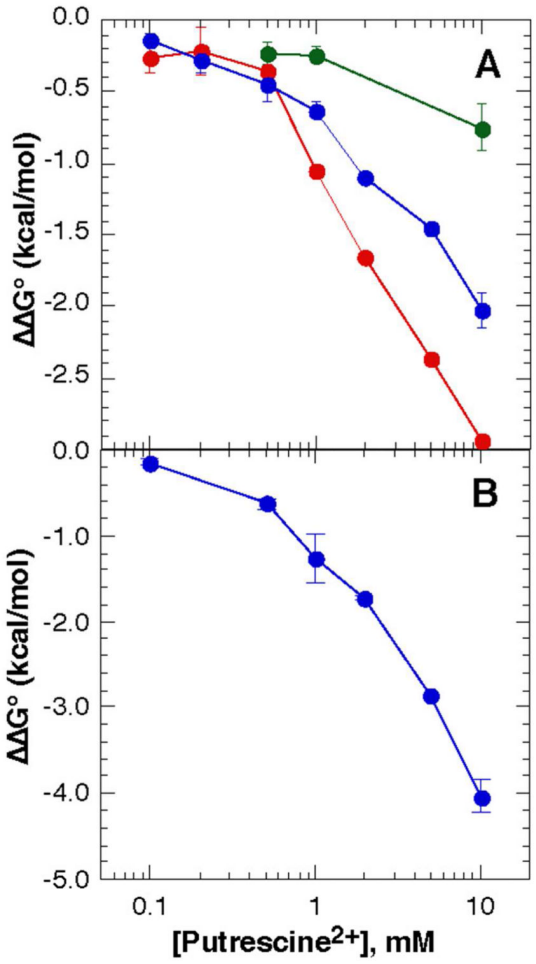

Figure 4.

Effect of putrescine^{2+} on the stability of RNAs without Mg^{2+} chelation sites. $\Delta\Delta G°_{obs}$ for both RNAs was measured in K•MOPS - EDTA buffer with 50 mM K^+ and 0.1 mM (red), 0.2 mM (blue) or 0.5 mM (green) $MgCl_2$. 20 μM DAP was included with the A-riboswitch. **A**, A-riboswitch; **B**, TLR RNA.

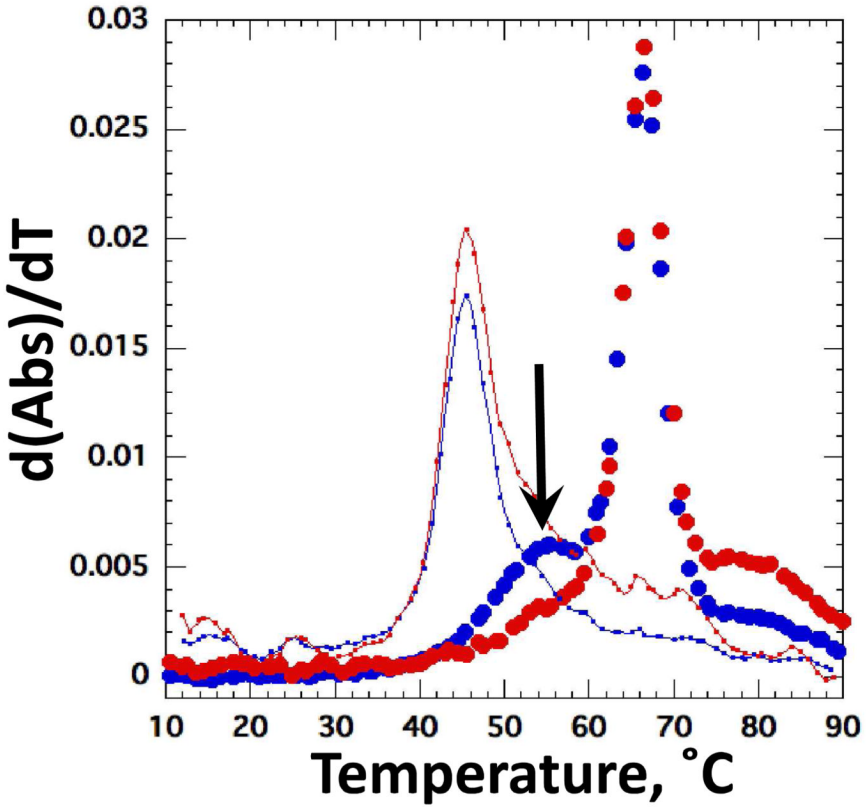

Figure 5.

Melting profile of the M-box riboswitch. Data are plotted as the derivative of absorbance with respect to temperature at 260 nm (blue) and 280 nm (red). Closed circles correspond to data collected in buffer with 50 mM K^+, 1 mM putrescine^{2+} and 1 mM Mg^{2+}, in K•MOPS – EDTA buffer. Solid lines correspond to data collected in the same buffer with 50 mM K^+ and no divalent ions. Arrow indicates new transition that appears in the presence of Mg^{2+}.

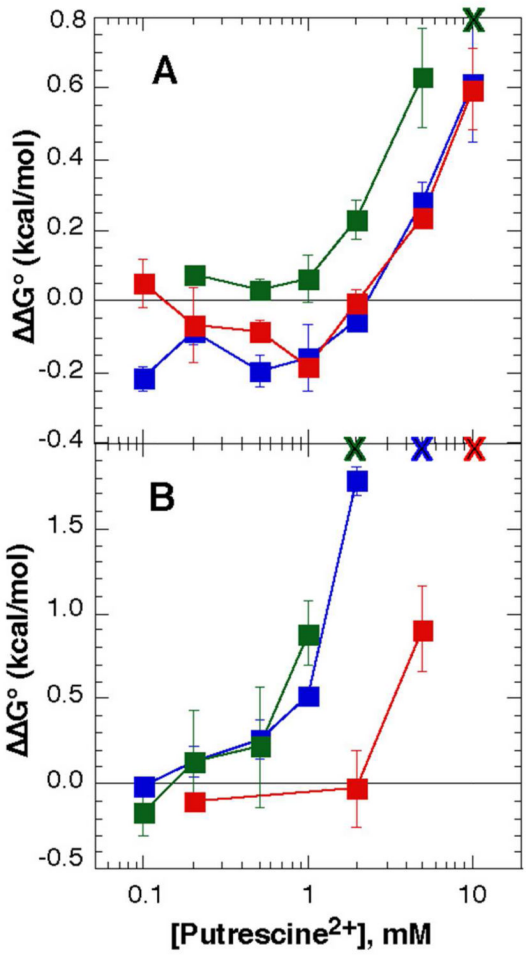

Figure 6.

Stability of the magnesium-chelating RNAs in varying concentrations of putrescine^{2+}. **A**, stability of the 58mer rRNA fragment relative to stability in buffer with 50 mM K^+ and 0.5 mM (green), 1.0 mM (blue), or 2.0 mM (red) $MgCl_2$. The green "X" at the top of the graph represents the concentration of putrescine^{2+} (with 0.5 mM Mg^{2+}) at which the tertiary structure can no longer be detected in the melting curves. **B**, stability of the M-box RNA relative to buffer with 50 mM K^+ and 0.75 mM (green), 1.0 mM (blue), or 2.0 mM (red) $MgCl_2$. An "X" at the top of graph represents the concentration of putrescine where the tertiary structure is no longer observed with 0.75 mM (green), 1 mM (blue), or 2 mM (red) Mg^{2+}.

Table 1

RNA stabilization by divalent ions[a]

RNA	divalent ion	pK_a [b]	$[2+]_0$, mM	$\Delta\Delta G°_{obs}$, max, kcal/mol	$\Delta\Gamma_{2+}$, ions/RNA
A-riboswitch	Mg^{2+}		0.104 ± 0.006	−7.30 ± 0.15	3.31 ± 0.20
A-riboswitch	putrescine	9.36 (9.35)	0.87 ± 0.57	−6.36 ± 0.14	2.39 ± 0.11
TLR RNA	Mg^{2+}		0.1.62 ± 0.31	−5.33 ± 0.43	2.06 ± 0.30
TLR RNA	putrescine		9.80 ± 3.21	−3.88 ± 0.99	1.66 ± 0.47
A-riboswitch	cadaverine	(10.05)	1.30 ±0.15	−5.83 ±0.26	2.16 ± 0.17
A-riboswitch	1,3 diaminopropane	(8.6)	0.42 ± 0.2	−6.99 ± 0.12	2.58 ± 0.13
A-riboswitch	*cis*-1,4 diaminobutene	8.78	0.65 ± 0.06	−7.19 ± 0.26	2.41 ± 0.21
A-riboswitch	*trans*-1,4 diaminobutene	8.93	0.89 ±0.04	−7.09 ± 0.10	2.36 ± 0.07

[a] $\Delta\Delta G°_{obs,\ max}$ and $[2+]_0$ are for fits of eq (4) to data shown in Figures 2 and 3A. $\Delta\Gamma_{2+}$ was calculated by eq (5). All diamino compounds shown have a +2 charge at the pH of the experiments (6.8).

[b] pK_a values are the observed macroscopic first acid dissociation constants for the diamino compounds. Values in parentheses were taken from the literature (49-51); other values were determined as described in Materials and Methods.